Dynamic Friction Models for Longitudinal Road/Tire Interaction: Theoretical Advances

C. Canudas-de-Wit
Laboratoire d'Automatique de Grenoble
UMR CNRS 5528
ENSIEG-INPG, B.P. 46
38 402 ST. Martin d'Hères, FRANCE
email: canudas@lag.ensieg.inpg.fr

P. Tsiotras and E. Velenis
School of Aerospace Engineering
Georgia Institute of Technology
Atlanta, GA 30332-0150, USA
email: p.tsiotras@ae.gatech.edu

ABSTRACT
In this paper we derive a new dynamic friction force model for the longitudinal road/tire interaction for wheeled ground vehicles. The model is based on a dynamic friction model developed previously for contact-point friction problems, called the LuGre model [1]. By assuming a contact patch between the tire and the ground we develop a partial differential equation for the distribution of the friction force along the patch. An ordinary differential equation (the lumped model) for the friction force is developed based on the patch boundary conditions and the normal force distribution along the contact patch.

KEY WORDS
Tire Friction, Dynamic Model, LuGre Model, ABS, TCS

1. Introduction

The problem of predicting the friction force between the tire and the ground for wheeled vehicles is of enormous importance to automotive industry. However, accurate tire/ground friction models are difficult to obtain analytically. Subsequently, in the past several years, the problem of modeling and predicting tire friction has become an area of intense research in the automotive community. In particular, Anti-lock Braking Systems (ABS) and Traction Control Systems (TCS) rely on knowledge of the friction characteristics. Such systems have enhanced safety and maneuverability to such an extend, that they have become almost mandatory for all future passenger vehicles.

The main difficulty in designing ABS and TCS systems is the nonlinearity and uncertainty of the tire/road models. In either case, the friction force at the tire/road interface is the main mechanism for converting wheel angular acceleration or deceleration (due to the motor torque or braking) to forward acceleration of deceleration (longitudinal force). Therefore, the study of the friction force characteristics at the road/tire interface is of paramount importance for the design of ABS and/or TCS systems.

A common assumption in most tire friction models is that the normalized tire friction μ

$$\mu = \frac{F}{F_n} = \frac{\text{Friction force}}{\text{Normal force}}$$

is a nonlinear function of the normalized relative velocity between the road and the tire (slip coefficient s) with a distinct maximum; see Fig. 1. In addition, it is understood that μ also depends on the velocity of the vehicle and road surface conditions, among other factors (see [2] and [3]). The curves shown in Fig. 1 illustrate how these factors influence the shape of μ.

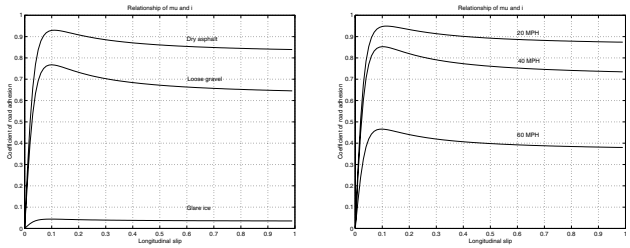

Figure 1. Typical variations of the tire/road friction profiles for different road surface conditions (left), and different vehicle velocities (right). Curves given by Harned et al. [3].

The curves shown in Fig. 1 are derived empirically, based solely on steady-state (i.e., constant linear and angular velocity) experimental data [3] in a highly controlled laboratory environment or using specially designed test vehicles. Under such steady-state conditions, experimental data seem to support the force vs. slip curves of Fig. 1. In reality, the linear and angular velocities can never be controlled independently and hence, such idealized steady-state conditions are not reached except during the rather uninteresting case of cruising with constant speed. The development of the friction force at the tire/road interface is very much a dynamic phenomenon. Experiments performed in commercial vehicles, have shown that the tire/road forces do not necessarily vary along the curves shown Fig. 1, but rather "jump" from one value to another when these forces are displayed in the $\mu - s$ plane [4]. In addition, in realistic situations, these variations are most likely to exhibit hysteresis loops, clearly indicating the dynamic nature of friction.

In this paper, we develop a new, velocity-dependent, dynamic friction model that can be used to describe the tire/road interaction. The proposed model has the advantage that is developed starting from first principles based on a simple, point-contact dynamic friction model [1]. The parameters entering the model have a physical significance

allowing the designer to tune the model parameters using experimental data. The proposed friction model is also velocity-dependent, a property that agrees with experimental observations. A simple parameter in the model can also be used to capture the road surface characteristics. Finally, in contrast to many other static models, our model is shown to be well-defined everywhere (even at zero rotational or linear vehicle velocities) and hence, is appropriate for any vehicle motion situations as well as for control law design. This is especially important during transient phases of the vehicle operation, such as during braking or acceleration.

2. Static slip/force models

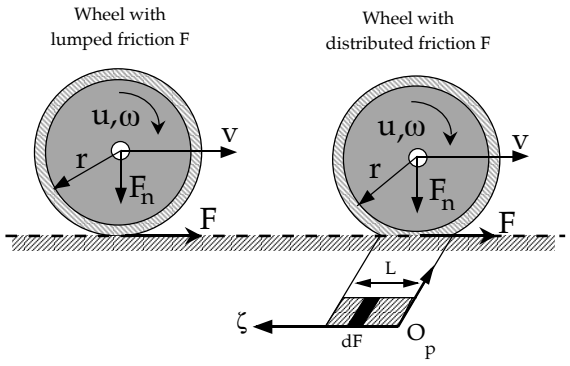

Figure 2. One-wheel system with lumped friction (left), and distributed friction (right).

The most common tire friction models used in the literature are those of algebraic slip/force relationships. They are defined as one-to-one (memoryless) maps between the friction F, and the longitudinal slip rate s, which defined as

$$s = \begin{cases} s_b = \dfrac{r\omega}{v} - 1 & \text{if} \quad v > r\omega, \;\; v \neq 0 \quad \text{for braking} \\ s_d = 1 - \dfrac{v}{r\omega} & \text{if} \quad v < r\omega, \;\; \omega \neq 0 \quad \text{for driving} \end{cases} \tag{1}$$

The absolute value of the slip rate is defined in the interval $[0, 1]$. When $s = 0$ there is no sliding (pure rolling), whereas $|s| = 1$ indicates full sliding/skidding. It should be pointed out that in this paper we always define the relative velocity as $v_r = r\omega - v$. As a result, the slip coefficient in (1) is positive for driving and negative for braking.

The slip/force models aim at describing the shapes shown in Fig. 1 via static maps $F(s) : s \mapsto F$. They may also depend on the vehicle velocity v, i.e. $F(s, v)$, and vary when the road characteristics change. Some of the most typical static models are the Pacejka's model (see, Pacejka and Sharp [5]), also known as the "Magic Formula" and the models by Burckhardt [2] and Kiencke and Daiss [6].

2.1 The Lumped LuGre Model

As an alternative to the static $F(s)$ maps dynamic models can be adopted. The so-called "dynamic friction models" attempt to capture the transient behavior of the tire-road contact forces under time-varying velocity conditions. Generally speaking, dynamic models can be formulated either as lumped or as distributed models, as shown in Fig. 2. A *lumped* friction model assumes a point tire-road friction contact. As a result, the mathematical model describing such a model is an ordinary differential equations that can be easily solved by time integration. *Distributed* friction models, on the other hand, assume the existence of a *contact patch* between the tire and the ground with an associated normal pressure distribution. This formulation results in a partial differential equation, that needs to be solved both in time and space [7].

A number of dynamic models have been proposed in the literature that can be classified under the term "dynamic friction models." One such model, for example, has been proposed by Bliman et al. in [7]. Another lumped dynamic model that can be used to accurately predict the friction forces during transients is the LuGre friction model [8].

The LuGre model is an extension of the Dahl model that includes the Stribeck effect (see, [1]). The lumped, LuGre model as proposed in [8, 9], is given as,

$$\dot{z} = v_r - \frac{\sigma_0 |v_r|}{g(v_r)} z \tag{2}$$

$$F = (\sigma_0 z + \sigma_1 \dot{z} + \sigma_2 v_r) F_n \tag{3}$$

with

$$g(v_r) = \mu_c + (\mu_s - \mu_c) e^{-|v_r/v_s|^\alpha} \tag{4}$$

where σ_0 is the rubber longitudinal lumped stiffness, σ_1 the rubber longitudinal lumped damping, σ_2 the viscous relative damping, μ_c the normalized Coulomb friction, μ_s the normalized static friction, ($\mu_c \leq \mu_s$), v_s the Stribeck relative velocity, F_n the normal force, $v_r = r\omega - v$ the relative velocity, and z the internal friction state. The constant parameter α is used to capture the steady-steady friction/slip characteristic[1].

3. The LuGre Distributed model

Distributed models assume the existence of an area of contact (or patch) between the tire and the road, as shown in Fig. 2. This patch represents the projection of the part of the tire that is in contact with the road. With the contact patch is associated a frame O_p, with ζ-axis along the length of the patch in the direction of the tire rotation. The patch length is L.

In order to extend the point friction model (2)-(3) to a distributed friction model we let $z(\zeta, t)$ denote the friction state (deflection) of the bristle/patch element located at the point ζ along the patch at a certain time t. The model (2)-(3) implies that

$$\frac{d\,z}{dt}(\zeta, t) = v_r - \frac{\sigma_0 |v_r|}{g(v_r)} z, \quad F = \int_0^L dF(\zeta, t)\,, \tag{5}$$

[1]The model in (3) differs from the point-contact LuGre model in [1] in the way that the function $g(v)$ is defined. Here we propose to use $\alpha = 1/2$ instead of $\alpha = 2$ as in the LuGre point-contact model in order to better match the pseudo-stationary characteristic of this model (map $s \mapsto F(s)$) with the shape of the Pacejka's model.

with $g(v_r)$ defined as in (4) and where

$$dF(\zeta,t) = \left(\sigma_0\, z(\zeta,t) + \sigma_1 \frac{\partial z}{\partial t}(\zeta,t) + \sigma_2 v_r\right) dF_n(\zeta,t)\,,$$

This model assumes that the contact velocity of each differential state element is equal to v_r.

Assuming a steady-state normal force distribution $dF_n(\zeta,t) = dF_n(\zeta)$ and introducing a normal force density function $f_n(\zeta)$ (force per unit length) along the patch, i.e., $dF_n(\zeta) = f_n(\zeta)d\zeta$ one obtains the total friction force as

$$F(t) = \int_0^L (\sigma_0 z(\zeta,t) + \sigma_1 \frac{\partial z}{\partial t}(\zeta,t) + \sigma_2 v_r) f_n(\zeta) d\zeta \quad (6)$$

Noting that[2] $\dot{\zeta} = |r\omega|$ we have that equation (5) describes a partial differential equation, i.e.

$$\frac{\partial\, z}{\partial \zeta}(\zeta,t)\,|r\omega| + \frac{\partial\, z}{\partial t}(\zeta,t) = v_r - \frac{\sigma_0 |v_r|}{g(v_r)}\, z(\zeta,t) \quad (7)$$

that should be solved in both in time and space.

3.1 Steady-State Characteristics

The time steady-state characteristics of the model (5) are obtained by setting $\frac{\partial z}{\partial \zeta}(\zeta,t) \equiv 0$ and by imposing that the velocities v and ω to be constant. Enforcing these conditions in (7) results in

$$\frac{\partial z(\zeta,t)}{\partial \zeta} = \frac{1}{|\omega r|}\left(v_r - \frac{\sigma_0 |v_r|}{g(v_r)} z(\zeta,t)\right) \quad (8)$$

At steady-state, v, ω (and hence v_r) are constant, and (8) can be integrated along the patch with the boundary condition $z(0,t) = 0$. A simple calculation shows that

$$z_{ss}(\zeta) \quad = \quad = c_2(1 - e^{c_1 \zeta}) \quad (9)$$

where $c_1 = -\frac{\sigma_0}{g(v_r)}\,\left|\frac{v_r}{\omega r}\right|$, $c_2 = \mathrm{sgn}(v_r)\frac{g(v_r)}{\sigma_0}$.

The steady-state value of the total friction force is calculated from (6)

$$F_{ss} = \int_0^L (\sigma_0 z_{ss}(\zeta) + \sigma_2 v_r) f_n(\zeta) d\zeta \quad (10)$$

To proceed with the calculation of F_{ss} we need to postulate a distribution for the normal force $f_n(\zeta)$. The typical form of the normal force distribution reported in the literature [10, 11], is shown in Fig. 3. However, for the sake of simplicity, other forms can be adopted. Some examples are given next.

- *Constant norm distribution.* A simple result can be derived if we assume uniform load distribution, as done in [8] and [12]. For uniform normal load

$$f_n(\zeta) = \frac{F_n}{L}, \quad 0 \le \zeta \le L \quad (11)$$

[2] It is assumed here that the origin of the ζ-frame changes location when the wheel velocity reverses direction, such that $\dot{\zeta} = r\omega$, for $\omega > 0$, and $\dot{\zeta} = -r\omega$, for $\omega < 0$.

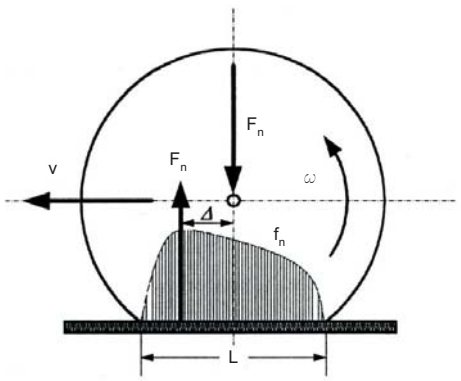

Figure 3. Typical normal load distribution along the patch; taken from [11].

and one obtains,

$$F_{ss} = \Big(\mathrm{sgn}(v_r) g(v_r)\Big[1 - \frac{Z}{L}(1 - e^{-L/Z})\Big] + \sigma_2 v_r\Big)\, F_n \quad (12)$$

where $Z = |\omega r| g(v_r)/|v_r|\,(\sigma_0)$.

- *Exponentially decreasing distribution.* In this case, the decrease of the normal load along the patch shown in Fig. 3 is approximated with an exponentially decreasing function

$$f_n(\zeta) = e^{-\lambda(\frac{\zeta}{L})} f_{n0}, \qquad 0 \le \lambda,\ \ 0 \le \zeta \le L \quad (13)$$

where $f_n(0) = f_{n0}$. This particular choice will become clear later on, when we reduce the infinite dimension distributed model to a simple lumped one having only one state variable. Moreover, for $\lambda > 0$ we have a strictly decreasing function of f_n. With the choice (13) one obtains

$$F_{ss} = \sigma_0 c_2 k_1 \Big(1 - e^{-\lambda} + k_2 e^{(-\lambda + CL)} + k_2\Big) + \sigma_2 v_r k_1 (1 - e^{-\lambda}) \quad (14)$$

where $k_1 = \frac{f_{n0} L}{\lambda}$, $k_2 = \frac{\lambda}{c_1 L - \lambda}$ and $f_{n0} = F_n \lambda/(1 - e^{-\lambda})L$.

- *Distributions with zero boundary conditions.* As shown in Fig. 3, a realistic force distribution has, by continuity, zero values for the normal load at the boundaries of the patch. Several forms satisfy this constraint. Some possible examples proposed herein are given below:

$$f_n(\zeta) = \tfrac{3F_n}{2L}\left[1 - \left(\tfrac{\zeta - L/2}{L/2}\right)^2\right] \quad (15a)$$

$$f_n(\zeta) = \tfrac{\pi F_n}{2L}\,\sin(\pi\zeta/L) \quad (15b)$$

$$f_n(\zeta) = \tfrac{\gamma^2 L^2 + \pi^2}{\pi L(e^{-\gamma L} + 1)}\exp^{-\gamma\zeta}\sin(\pi\zeta/L) \quad (15c)$$

where (15a), (15b) and (15c) describe a parabolic, sinusoidal and sinusoidal/exponential distributions, respectively.

where F_n denotes the total normal load.

3.2 Relation with the Magic Formula

The previously derived steady-state expressions, depend on both v and ω. They can also be expressed as a function of s and either v or ω. For example, for the constant distribution case, we have that $F_{ss}(s)$, can be rewritten as:

- *Driving case.* In this case $v < r\omega$, see also (1), and the force at steady-state is given by

$$F_d(s) = \mathrm{sgn}(v_r) F_n g(s) \left(1 + \frac{g(s)}{\sigma_0 L|s|}(e^{-\frac{\sigma_0 L|s|}{g(s)}} - 1)\right) + F_n \sigma_2 r\omega s \tag{16}$$

  with $g(s) = \mu_c + (\mu_s - \mu_c)\, e^{-|r\omega s/v_s|^\alpha}$, for some constant ω, and $s = s_d$.

- *Braking case.* The steady-state friction force for the braking case can be written as

$$F_b(s) = \mathrm{sgn}(v_r) F_n g(s) \left(1 + \frac{g(s)|1+s|}{\sigma_0 L|s|}(e^{-\frac{\sigma_0 L|s|}{g(s)|1+s|}} - 1)\right) + F_n \sigma_2 v s \tag{17}$$

  where $g(s) = \mu_c + (\mu_s - \mu_c)\, e^{-|vs/v_s|^\alpha}$, for constant v, and $s = s_b$; see also (1).

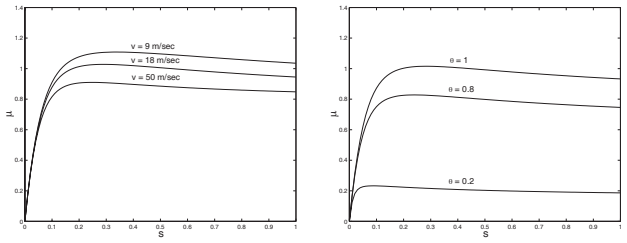

Figure 4. Static view of the distributed LuGre model with uniform force distribution (braking case) under: (left) different values for v, (right) different values for θ with $v = 20\,\mathrm{m/s} = 72\,\mathrm{Km/h}$. These curves show the normalized friction $\mu = F(s)/F_n$, as a function of the slip velocity s.

3.3 Dependency on Road Conditions

The level of tire/road adhesion, can be modeled by introducing a multiplicative parameter θ in the function $g(v_r)$. To this aim, we substitute $g(v_r)$ by

$$\tilde{g}(v_r) = \theta g(v_r)\,,$$

where $g(v_r)$ is the nominal known function given in (4). Computation of the function $F(s,\theta)$ as a function of θ, gives the curves shown in Fig. 4(b). These curves match reasonably well the experimental data shown in Fig. 1(a), for several coefficients of road adhesion. Hence, the parameter θ, can suitably describe the changes in the road characteristics.

We also note that the steady-state representation of the equations (16) or (17) can be used to identify most of the model parameters by fitting this model to experimental data. These parameters can also be used in a simple one-dimensional lumped model, which can be shown to suitably approximate the (average) solution of the partial differential equation (5). This approximation is discussed next.

4. Average Lumped Model

The disadvantage of a distributed model is that it requires a possibly large number of states to describe the friction generated at each tire. Alternatively, one could define a *mean friction state* $\bar{z}$ for each tire and then derive an *ordinary differential equation* for $\bar{z}$. This will simplify the analysis and can also lead to much simpler control design synthesis procedures for tire friction problems.

To this end, let us define

$$\bar{z}(t) \equiv \frac{1}{F_n}\int_0^L z(\zeta,t) f_n(\zeta) d\zeta \tag{18}$$

where F_n is the total normal force, given by $F_n = \int_0^L f_n(\zeta)\, d\zeta$. Thus,

$$\dot{\bar{z}}(t) = \frac{1}{F_n}\int_0^L \frac{\partial z}{\partial t}(\zeta,t) f_n(\zeta) d\zeta \tag{19}$$

Using (7) we get

$$\begin{aligned}\dot{\bar{z}}(t) &= \frac{1}{F_n}\int_0^L \left(v_r - \frac{\sigma_0|v_r|}{g(v_r)} z(\zeta,t) - \frac{\partial z(\zeta,t)}{\partial \zeta}|\omega r|\right) f_n(\zeta) d\zeta \\ &= v_r - \frac{\sigma_0|v_r|}{g(v_r)}\bar{z}(t) - \frac{|\omega r|}{F_n}\Big[z(\zeta,t) f_n(\zeta)\Big]_0^L \\ &\quad + \frac{|\omega r|}{F_n}\int_0^L z(\zeta,t)\frac{\partial f_n(\zeta)}{\partial \zeta} d\zeta\end{aligned}$$

The term in the square brackets describes the influence of the boundary conditions, whereas the integral term accounts for the particular form of the force distribution.

From (6) the friction force is

$$\begin{aligned}F(t) &= \int_0^L \left(\sigma_0\, z(\zeta,t) + \sigma_1 \frac{\partial z}{\partial t}(\zeta,t) + \sigma_2 v_r\right) f_n(\zeta)\; d\zeta \\ &= (\sigma_0 \bar{z}(t) + \sigma_1 \dot{\bar{z}}(t) + \sigma_2 v_r)\; F_n\end{aligned}$$

As a general goal, one wishes to introduce normal force distributions, that leads to the following form for the lumped LuGre model,

$$\dot{\bar{z}}(t) = v_r - \frac{\sigma_0|v_r|}{g(v_r)}\bar{z}(t) - \kappa(t)|\omega r|\bar{z}(t) \tag{20}$$

$$F(t) = (\sigma_0 \bar{z}(t) + \sigma_1 \dot{\bar{z}}(t) + \sigma_2 v_r)\, F_n \tag{21}$$

where $\kappa(t)$ is defined as:

$$\kappa(t) = \frac{1}{F_n\, \bar{z}}\left\{\Big[z(\zeta,t) f_n(\zeta)\Big]_0^L - \int_0^L z(\zeta,t)\frac{\partial f_n(\zeta)}{\partial \zeta} d\zeta\right\} \tag{22}$$

and F_n as above. When comparing this model with the point contact LuGre model (2)-(3), it is clear that κ captures the distributed nature of the former model. It is also expected that $\kappa > 0$, so that the map $v_r(t) \mapsto F(t)$ preserves the passivity properties of the point contact LuGre model [1].

For the case of normal load distributions with zero boundary conditions we have $f_n(0) = f_n(L) = 0$ and equation (22) yields

$$\kappa(t) = -\frac{\int_0^L z(\zeta,t) f_n'(\zeta) d\zeta}{\int_0^L z(\zeta,t) f_n(\zeta) d\zeta} \tag{23}$$

where $f_n'(\zeta) = \partial f_n(\zeta)/\partial\zeta$.

4.1 Influence of Force Distribution on $\kappa(t)$

Depending on the postulated normal force distribution density function, several expressions for the average lumped model can be developed. For instance, κ may be a constant, an explicit or an implicit function of the mean friction state $\bar{z}$. We study some of these forms next.

Parabolic Distribution: For a parabolic normal force distribution $f_n(\zeta)$ is given by (15a). In order to compute κ from (23) we now make the assumption that $z(\zeta,t)$ is a separable function of ζ and t, namely, $z(\zeta,t) = \varphi(\zeta)\theta(t)$ for some (time-independent) deflection function $\varphi(\zeta)$, $0 \le \zeta \le L$ and some (space-independent) time function $\theta(t)$, $t \ge 0$. From the previous discussion $\varphi(\zeta)$ can be interpreted as the deflection of the bristle along the patch at position ζ. We impose the boundary condition that $\varphi(0) = 0$, since there is no deflection for the first bristle element. Under the reasonable assumption that the deflection of the bristles builds gradually along the patch, we postulate that $\varphi(\zeta) = \zeta$ and hence

$$\kappa = -\frac{\int_0^L \varphi(\zeta)\theta(t) f_n'(\zeta) d\zeta}{\int_0^L \varphi(\zeta)\theta(t) f_n(\zeta) d\zeta} = -\frac{\int_0^L \zeta f_n'(\zeta) d\zeta}{\int_0^L \zeta f_n(\zeta) d\zeta} \tag{24}$$

A direct calculation gives that

$$\int_0^L \zeta f_n(\zeta) d\zeta = F_n \frac{L}{2} \qquad \text{and} \qquad \int_0^L \zeta f_n'(\zeta) d\zeta = -F_n \tag{25}$$

where $f_n(\zeta)$ as in (15a). Finally, $\kappa = \frac{2}{L}$. A more realistic model will assume that the deflection builds gradually but the rate of deflection build-up is reduced along the patch. This effect can be modeled by choosing $\varphi(\zeta) = \zeta^{\frac{1}{2}}$. Using such a φ and repeating the previous steps, one computes that $\kappa = \frac{7}{6}\frac{1}{L} \approx 1.1667\frac{1}{L}$. A more accurate estimate of κ can be computed assuming that the contact patch is divided into two separate regions, the sliding region and the adhesive region [10]. The sliding region can be modeled by linear bristle deflection. In the adhesive region the deflection of the bristles has reached a maximum and hence it stays constant. Therefore, we can choose the deflection function as $\varphi(\zeta) = b\,\mathrm{sat}(\zeta/b)$, where $0 < b < 1$ is a parameter that determines the transition between the sliding and adhesive regions of the contact patch. Using this expression for φ and tracing the same steps as before, one obtains the following value of κ as a function of the parameter b

$$\kappa = \frac{2b(3-2b)}{L\,(b^3 - 2b^2 + 2)} \tag{26}$$

This expression is shown in Fig. 5(a). A comparison of

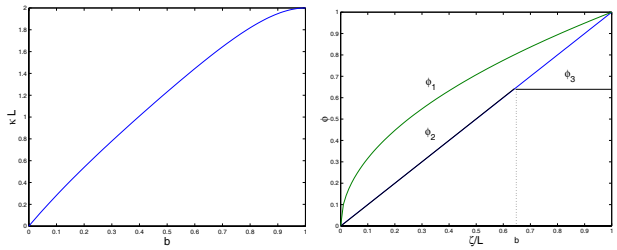

Figure 5. (left): Variation of κL with b. Realistically, b varies between $0.3 \le b \le 0.9$. (right): Comparison of bristle deflection distribution function $\varphi(\zeta)$ along the patch for $\varphi_1 = \zeta^{\frac{1}{2}}$, $\varphi_2(\zeta) = \zeta$, $\varphi_3(\zeta) = b\,\mathrm{sat}(\zeta/b)$.

several candidates for the bristle deflection function φ are shown in Fig. 5(b). Several other choices of the bristle deflection function $\varphi(\zeta)$ and the normal load distribution function $f_n(\zeta)$ can be used, yielding similar results. For most cases it is reasonable to chose κ in (20) to be a constant, somewhere in the range $1/L \le \kappa \le 2/L$.

Exponentially Decreasing Distribution: Assuming (13) along with $z(0,t) = 0$ one obtains

$$\kappa(t) \;=\; \frac{1}{F_n \bar{z}} z(L,t) e^{-\lambda} f_{n0} + \frac{\lambda}{L} \tag{27}$$

Next, recall that we require $\lambda \ge 0$. For large values of λ it is possible to ignore the term containing $z(L,t)$ in the equation above, and approximate $\kappa(t)$ by a constant $\kappa = \frac{\lambda}{L}$, wit $0 \le \lambda$.

Uniform Normal Distribution The case of the uniform normal distribution can be viewed as a special case of (13) with $\lambda = 0$. In this case $f_n(\zeta) = f_{n0} = F_n/L$ and we obtain the following expression

$$\kappa(t) = \frac{1}{F_n \bar{z}}\, z(L,t) f_{n0} = \frac{1}{L\bar{z}}\, z(L,t) \tag{28}$$

Deur [12] proposed that the boundary condition for the last element $z(L,t)$ be approximated by a linear expression of the average deflection $\bar{z}$, $z(L,t) \approx \kappa_0(t)\bar{z}$ resulting in the relation, $\kappa(t) = \kappa_0(t)/L$. The function $\kappa_0(t)$ is chosen in [12] so that the steady state solutions of the total friction force for the average/lumped model in (20)-(21), and the one of the distributed model (12) are the same. This approximation results in the following expression for κ_0

$$\kappa_0 = \kappa_0(Z) = \frac{1 - e^{-L/Z}}{1 - \frac{Z}{L}(1 - e^{-L/Z})} \tag{29}$$

In [12] it is also shown that, such a κ_0 belongs to the range $1 \leq \kappa_0(t) \leq 2$ for all $t \geq 0$. Often, a constant value for $\kappa_0 \in [1, 2]$ can be chosen, without significantly changing the steady states of the distributed and lumped models. This can be verified from Fig. 6. Interestingly, this range of κ_0 is in agreement with the results of a parabolic normal load distribution; see Fig. 5(a).

The plots 6 show the steady-state friction force as a function of the slip coefficient for the distributed model with uniform (Fig. 6(a)) and non-uniform normal load distribution (Fig. 6(b)), along with the steady-state plots of both average models.For comparison, a fit with the Pacejka's "Magic Formula" is also shown.

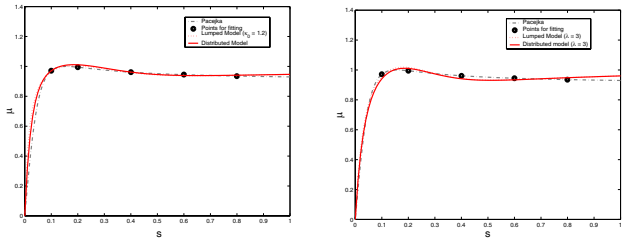

Figure 6. Steady-state plots assuming: (left) uniform normal load distribution using the approximation from [12] with $\kappa_0 = 1.2$, and (right) the non-uniform normal load distribution given in (13) with $\lambda = 3$.

5. Conclusions

In this paper we have revisited the problem of characterizing the friction at the tire/surface interface for wheeled vehicles. We have shown that static friction models are inadequate for describing the transient nature of friction build-up. Dynamic friction models are thus necessary to capture such transients during abrupt braking and acceleration phases. We propose a new dynamic friction model that accurately captures friction transients, as well as velocity-dependent characteristics and tire/road properties. The model is developed by extending the well-known LuGre point friction model to the case of a contact patch at the tire/surface interface. Contrary to common static friction/slip maps, it is shown that this new dynamic friction model is able to accurately capture the transient behavior of the friction force observed during transitions between braking and acceleration.

Acknowledgements: The first two authors would like to acknowledge support from CNRS and NSF (award No. INT-9726621/INT-9996096). The second author gratefully acknowledges partial support from the US Army Research Office under contract No. DAAD19-00-1-0473.

References

[1] Canudas de Wit, C., Olsson, H., Åström, K.J., and Lischinsky, P., A New Model for Control of Systems with Friction, *IEEE Transactions on Automatic Control*, Vol. 40, No. 3, 1995, 419–425.

[2] Burckhardt, M., *Fahrwerktechnik: Radschlupfregelsysteme*, (Vogel-Verlag, Germany, 1993).

[3] Harned, J., Johnston, L. and Scharpf, G., Measurement of Tire Brake Force Characteristics as Related to Wheel Slip (Antilock) Control System Design, *SAE Transactions*, Vol. 78, Paper 690214, 1969, 909–925.

[4] van Zanten, A., Ruf, W.D., and Lutz, A., Measurement and Simulation of Transient Tire Forces, In *International Congress and Exposition*, Detroit, MI, SAE Technical Paper Series, Paper 890640, 1989.

[5] Pacejka, H.B. and Sharp, R.S., Shear Force Developments by Pneumatic Tires in Steady-State Conditions: A Review of Modeling Aspects, *Vehicle Systems Dynamics*, Vol. 20, 1991, 121–176.

[6] Kiencke, U. and Daiss, A., Estimation of Tyre Friction for Enhaced ABS-Systems, In *Proceedings of the AVEG'94*, 1994.

[7] Bliman, P.A., Bonald, T. and Sorine, M., Hysteresis Operators and Tire Friction Models: Application to Vehicle Dynamic Simulations, *Proc. of ICIAM'95*, Hamburg, Germany, 3-7 July, 1995.

[8] Canudas de Wit, C. and Tsiotras, P., Dynamic Tire Friction Models for Vehicle Traction Control, In *Proceedings of the IEEE Conference on Decision and Control*, Phoenix, AZ, 1999, 3746–3751.

[9] Canudas de Wit, C., Horowitz, R. and Tsiotras, P., Model-Based Observers for Tire/Road Contact Friction Prediction, In *New Directions in Nonlinear Observer Design*, Nijmeijer, H. and T.I Fossen (Eds), Springer Verlag, Lectures Notes in Control and Information Science, May 1999.

[10] Wong J.Y., *Theory of Ground Vehicles*, (New York: John Wiley & Sons, Inc., 1993).

[11] Gim, G. and Nikravesh, P.E., A Unified Semi-Empirical Tire Model with Higher Accuracy and Less Parameters, *SAE International Congress and Exposition*, Detroit, MI, 1999.

[12] Deur, J., Modeling and Analysis of Longutudinal Tire Dynamics Based on the LuGre Friction Model, In *Proceedings of the IFAC Conference on Advances in Automotive Control*, Kalsruhe, Germany, 2001, 101–106.